

## Compositional dependence of optical critical point parameters in pseudomorphic GeSn alloys

Vijay Richard D'Costa,<sup>1</sup> Wei Wang,<sup>1</sup> Qian Zhou,<sup>1</sup> Taw Kuei Chan,<sup>2</sup> Thomas Osipowicz,<sup>2</sup> Eng Soon Tok,<sup>2</sup> and Yee-Chia Yeo<sup>1</sup>

<sup>1</sup>Department of Electrical and Computer Engineering, National University of Singapore, Singapore 117583

<sup>2</sup>Department of Physics, National University of Singapore, Singapore 117551

(Received 5 June 2014; accepted 23 July 2014; published online 5 August 2014)

Spectroscopic ellipsometry was used to investigate the optical response of pseudomorphic  $\text{Ge}_{1-x}\text{Sn}_x$  ( $0 \leq x \leq 0.17$ ) alloys grown directly on Ge (100) by molecular beam epitaxy. A detailed compositional study of amplitudes, broadenings, energies, and phase angles associated with critical points  $E_1$ ,  $E_1 + \Delta_1$ ,  $E'_0$ , and  $E_2$  of GeSn alloys was carried out using a derivative analysis. The results can be understood in terms of the electronic bandstructure of Ge or relaxed GeSn alloys with the following differences. First, broadening parameters in pseudomorphic alloys are found to have lower values compared to relaxed alloys indicating lower dislocation density in our pseudomorphic alloys relative to relaxed alloys. Second, the amplitudes of  $E_1$  and  $E_1 + \Delta_1$  are enhanced and reduced, respectively, with respect to relaxed GeSn alloys, and the trends are captured using the  $k \cdot p$  method as a biaxial stress induced effect. Third, phase angles are lower than Ge for all the critical points suggesting reduction of excitonic effects in GeSn with respect to Ge.

© 2014 AIP Publishing LLC. [<http://dx.doi.org/10.1063/1.4892105>]

### I. INTRODUCTION

The recent availability of high quality GeSn alloys grown by chemical vapour deposition (CVD)<sup>1–3</sup> and molecular beam epitaxy (MBE)<sup>4–8</sup> has made possible the study of their interesting optical properties which are of scientific and technological importance. A systematic study of compositional dependence of dielectric function and critical point energies  $E_0$ ,  $E_1$ ,  $E_1 + \Delta_1$ ,  $E'_0$ , and  $E_2$  is available for relaxed  $\text{Ge}_{1-x}\text{Sn}_x$  alloys grown by CVD.<sup>2</sup> Large bowing in the compositional dependence of energies was determined for all the critical points in relaxed  $\text{Ge}_{1-x}\text{Sn}_x$  alloys. One important result that came out from that study was the possibility that the Sn concentration  $x_c$  needed to achieve a direct bandgap  $\text{Ge}_{1-x}\text{Sn}_x$  could be as low as  $\sim 0.06$  compared with the theoretical estimate of  $\sim 0.20$  at that time. Subsequent theoretical calculations and recent experimental work support the new indirect-direct crossover close to  $x_c$ .<sup>7,9,10</sup> GeSn alloys are now being pursued for applications in optoelectronics and nanoelectronics. Optical devices such as photodetectors and light emitting diodes have been fabricated.<sup>11–13</sup> Metal-oxide-semiconductor field-effect transistors (MOSFETs) based on GeSn have also been realized.<sup>14–16</sup> In particular,  $p$ -MOSFETs with biaxially strained GeSn as the channel material enhance the mobility with respect to Ge. Although recent theoretical calculations<sup>17</sup> predict that compressively strained GeSn alloys could be direct bandgap for  $x_c \sim 0.1$ , experimental data<sup>18</sup> suggest that  $x_c$  could be as high as 0.17. It must be pointed out that range of Sn concentration needed to accomplish a direct bandgap in compressively strained GeSn is still subject to further experimental investigation.<sup>19</sup>

Previous reports on MBE-grown GeSn alloys have mainly focused on the indirect bandgap and the lowest direct bandgap.<sup>7,20,21</sup> Recently, we reported a preliminary study on

above-band gap optical properties of biaxially strained GeSn alloys.<sup>6</sup> The dielectric function of pseudomorphic alloys indicated Ge-like bandstructure. The presence of compressive strain causes a blue-shift in  $E_1$ ,  $E_1 + \Delta_1$ ,  $E'_0$ , and  $E_2$  of pseudomorphic alloys with respect to their relaxed counterparts.

Critical point analysis of dielectric function gives four parameters: amplitudes, broadenings, energies, and phase angles for each transition.<sup>22</sup> These parameters contain rich information about the electronic bandstructure of a material. Experimental study of energy and broadening parameters in relaxed GeSn revealed interesting scaling behavior for the electronic properties in comparison with SiGe. It was found that the bowing in relaxed GeSn and SiGe alloys scale with the lattice mismatch and electronegativity mismatch.<sup>2</sup> We would like to investigate the impact of pseudomorphic strain in GeSn on amplitudes, broadenings, and phase angles in addition to transition energies. Interesting polarization dependence of amplitude parameters for  $E_1$  and  $E_1 + \Delta_1$  critical points is observed in bulk Ge subject to uniaxial stress depending on whether the light is polarized parallel or perpendicular to applied stress.<sup>23</sup> Broadening parameters are affected by temperature, doping, and the alloying effect. Broadening parameter for  $E_1$  is also found to be sensitive to the dislocation density in group-IV alloys.<sup>24</sup> Pseudomorphic SiGeC alloys which have lower dislocation density than relaxed alloys show narrow broadening parameters. Phase angle is related to the geometrical nature of a critical point and is also assumed to capture the many body effects.<sup>22</sup> Excitonic effects are shown to be important in the electronic bandstructure calculations of bulk Si, which is representative for group-IV semiconductors.<sup>25</sup> The agreement between the theoretical and experimental dielectric functions of Si was much better with the inclusion of excitonic effects. Phase

angles for  $E_1$  and  $E_1 + \Delta_1$  did not show any stress dependence for Ge (Ref. 23), and they are yet to be reported for GeSn alloys. Amplitudes have been reported for relaxed GeSn alloys but only for  $E_1$  and  $E_1 + \Delta_1$ .

In this paper, we report the compositional dependence of amplitudes, broadenings, phase, and energies for all four critical points  $E_1$ ,  $E_1 + \Delta_1$ ,  $E'_0$ , and  $E_2$  in pseudomorphic GeSn alloys. Spectroscopic ellipsometry was used to determine the dielectric function of  $\text{Ge}_{1-x}\text{Sn}_x$  ( $0 \leq x \leq 0.17$ ) alloys from 1.3 to 4.7 eV. The experimental results reveal electronic band-structure very similar to Ge or relaxed GeSn alloys. We find that the critical point transitions show narrower broadenings compared to relaxed alloys indicating lower dislocation density in pseudomorphic alloys with respect to relaxed alloys. The amplitudes for  $E_1$  and  $E_1 + \Delta_1$  in pseudomorphic GeSn appear to be affected by the presence of biaxial stress. Amplitude for  $E_1$  is enhanced whereas the amplitude for  $E_1 + \Delta_1$  is reduced with respect to relaxed GeSn alloy, which is consistent with predictions using the  $k \cdot p$  method.

## II. GROWTH DETAILS AND STRUCTURAL CHARACTERIZATION

The growth of  $\text{Ge}_{1-x}\text{Sn}_x$  ( $0 \leq x \leq 0.17$ ) films on Ge (100) substrates was performed in a solid-source MBE system with a base pressure of  $3 \times 10^{-10}$  Torr located at the National University of Singapore (NUS). The details about GeSn growth are described in Ref. 6. We produced a number of pseudomorphic GeSn films with thicknesses ranging from 200 nm to 25 nm as  $x$  varied from 0.02 to 0.17. As previously reported for pseudomorphic  $\text{Ge}_{1-x}\text{Sn}_x$  alloys,<sup>4</sup> the critical thickness to obtain high quality or pseudomorphic alloys decreases as a function of  $x$ .

The samples were investigated for their crystalline quality, composition, strain, and thickness by high-resolution x-ray diffractometry (HR-XRD), Rutherford backscattering (RBS), and cross-sectional transmission electron microscopy (XTEM). HR-XRD (004)  $\omega$ - $2\theta$  curves for all samples showed Pendellösung fringes indicating coherent epitaxial films.<sup>6</sup> Figure 1(a) shows the (004)  $\omega$ - $2\theta$  scan and a  $(\bar{2}06)$  reciprocal space mapping (RSM) for a  $\text{Ge}_{0.975}\text{Sn}_{0.025}$  alloy. The presence of pseudomorphic strain in our alloys was confirmed by RSM, from which the Sn composition  $x$  and in-plane strain  $\varepsilon_{\parallel}$  are determined. We adopted the following procedure to determine  $x$ , which was subsequently used in the calculation of  $\varepsilon_{\parallel}$ : Out-of-plane lattice constant  $a_{\perp}$  and in-plane lattice constant  $a_{\parallel}$  of  $\text{Ge}_{1-x}\text{Sn}_x$  are obtained from the ratio of Ge to GeSn RSM peaks of  $Q_{\perp}$  and  $Q_{\parallel}$ , respectively.  $Q_{\parallel}$  and  $Q_{\perp}$  are the reciprocal vectors along [110] and [001] and are expressed in reciprocal lattice units (rlu). The relaxed lattice constant<sup>26</sup>  $a$  of GeSn is calculated from  $a_{\parallel}$  and  $a_{\perp}$  with Ge values for  $c_{11}$  and  $c_{12}$  (Ref. 27) as the starting values. The experimental  $a$  of pseudomorphic GeSn alloys<sup>4</sup> follows Vegard's law  $(1-x)a_{\text{Ge}} + xa_{\text{Sn}}$ , from which the preliminary  $x$  is extracted. This preliminary  $x$  is then used to re-calculate  $a$  from  $a_{\perp}$  to  $a_{\parallel}$ , but now with composition weighted average values of Ge and  $\alpha$ -Sn for  $c_{11}$  and  $c_{12}$ . Vegard's law for  $a$  then gives us our value of  $x$ . We must point out that although the use of Ge values for  $c_{11}$  and  $c_{12}$

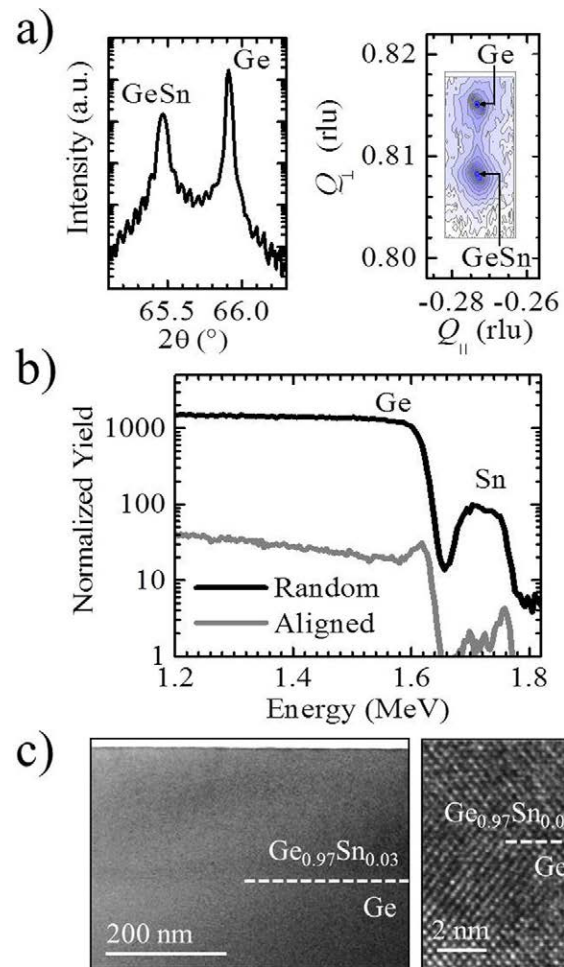


FIG. 1. (a) HRXRD (004)  $\omega$ - $2\theta$  scan and  $(\bar{2}06)$  RSM of a  $\text{Ge}_{0.975}\text{Sn}_{0.025}$  alloy. Both Ge and GeSn peaks have the same  $Q_{\parallel}$  indicating that the epitaxial GeSn layer is fully strained to Ge. The wavelength of X-ray radiation used was 1.538 Å. (b) 2 MeV  $\text{He}^+$  RBS random and [100] axial channelled spectra for a  $\text{Ge}_{0.971}\text{Sn}_{0.029}$  alloy. (c) Low magnification XTEM image for a  $\text{Ge}_{0.971}\text{Sn}_{0.029}$  alloy. The inset shows a sharp interface between  $\text{Ge}_{0.971}\text{Sn}_{0.029}$  and Ge indicating good crystalline quality of GeSn epitaxially grown on Ge.

overestimates  $x$ , it only leads to a maximum deviation of  $\sim 0.2\%$  for  $\text{Ge}_{0.83}\text{Sn}_{0.17}$  with respect to its final value. The Sn composition obtained from XRD was verified by RBS in a few alloys. Figure 1(b) shows the elemental distribution obtained from RBS for a  $\text{Ge}_{0.971}\text{Sn}_{0.029}$  alloy. The XTEM data shown in Fig. 1(c) for  $\text{Ge}_{0.971}\text{Sn}_{0.029}$  indicated that the film is of uniform thickness with a sharp interface between the film and the substrate. The inset shows a virtually defect-free interface between GeSn and Ge. The surface quality of GeSn films was investigated by atomic force microscopy (AFM), which showed that the root mean square (RMS) roughness is less than 1 nm for all our samples. Table I provides a summary of growth and structural parameters for pseudomorphic GeSn alloys.

## III. OPTICAL PROPERTIES

### A. Ellipsometric measurements and data processing

Spectroscopic ellipsometry measurements were performed on a rotating analyzer ellipsometer from J. A. Woollam Co.<sup>28</sup>

TABLE I. Growth and structural parameters for pseudomorphic  $\text{Ge}_{1-x}\text{Sn}_x$  alloys.  $a_{\parallel} = a_{\text{Ge}} = 5.658 \text{ \AA}$  and  $a_{\text{Sn}} = 6.491 \text{ \AA}$ .

$x$ (%)	$t$ (nm)	Growth temperature ( $^{\circ}\text{C}$ )	Growth rate (nm/min)	$a_{\perp}$ ( $\text{\AA}$ )	$\epsilon_{\parallel}$ (%)
0	175	170	$\sim 1.7$	5.658	0
2.0	125	170	$\sim 1.7$	5.686	-0.3
2.5	200	170	$\sim 1.7$	5.694	-0.4
3.9	50	170	$\sim 1.7$	5.715	-0.6
5.9	158	170	$\sim 1.7$	5.743	-0.9
8.4	104	170	$\sim 1.8$	5.780	-1.3
10.8	65	150	$\sim 1.8$	5.816	-1.6
16.6	25	100	$\sim 1.9$	5.901	-2.5

The ellipsometric angles  $\Psi$  and  $\Delta$  were measured at room temperature for two angles of incidence ( $65^{\circ}$  and  $75^{\circ}$ ) from 1.3 to 4.7 eV in 10 meV energy steps. A Ge film grown on Ge substrate was characterized along with the GeSn alloys as a reference sample. The optical response was modeled as originating from a three-layer system containing a Ge substrate, a GeSn film, and a  $\text{GeO}_2$  oxide layer.<sup>2</sup> The dielectric function of  $\text{GeO}_2$  oxide is known.<sup>29</sup> We determined the dielectric function of Ge substrate used in growth experiments separately and used it in a tabulated form in the model. The complex dielectric function of GeSn film is obtained by a point-by-point fit of  $\Psi$  and  $\Delta$ . We followed the procedure described in Ref. 2 for the extraction of Kramers-Kronig consistent dielectric function. We note that an isotropic dispersion model fully accounts for the observed dielectric response of pseudomorphic GeSn alloys although anisotropic optical response is expected in the presence of biaxial stress. This is because the acquired spectroscopic ellipsometry data correspond to the in-plane component of dielectric function for the experimental conditions used.<sup>30,31</sup>

## B. Dielectric function and critical point analysis

The dielectric function of GeSn alloys is shown in Fig. 2. The pseudomorphic alloys show sharp features in the dielectric function which are similar to the features observed in Ge dielectric function.<sup>22</sup> The dielectric function of alloys is red-shifted with respect to Ge with increasing Sn concentration indicating the alloying effect of Sn on the electronic bandstructure of pure Ge.<sup>2</sup> We determine the critical point parameters from a second-derivative analysis of measured dielectric function. Numerical differentiation of the complex dielectric function is carried out using 17 Savitzky-Golay coefficients for second-order derivatives with a polynomial of order 5.<sup>32,33</sup> We ensured that the number of smoothing coefficients used did not distort the line shape. We fitted the derivatives of the experimental dielectric function using<sup>2</sup>

$$\frac{d^2\epsilon}{dE^2} = \sum_j \frac{A_j e^{i\Phi_j}}{[E - E_j + i\Gamma_j]^2}, \quad (1)$$

where  $A_j$  is the amplitude for transition  $j$ ,  $\Phi_j$  is the phase angle,  $E_j$  is the critical point energy, and  $\Gamma_j$  is the broadening parameter. The summation covers the four critical points  $E_1$ ,  $E_1 + \Delta_1$ ,  $E'_0$ , and  $E_2$ . Both the imaginary and real

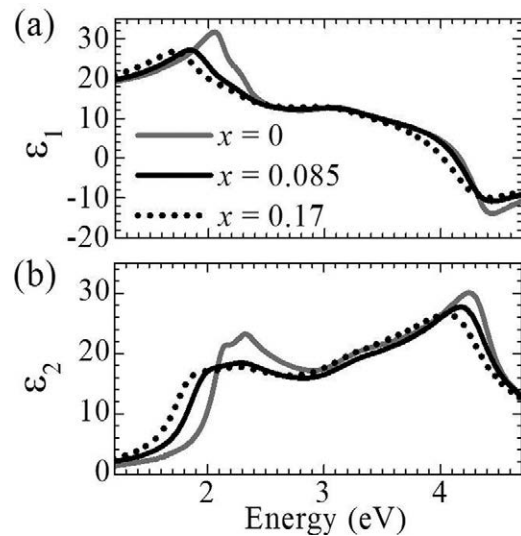


FIG. 2. (a) Real and (b) Imaginary parts of the complex dielectric function of  $\text{Ge}_{1-x}\text{Sn}_x$  alloys and a relaxed Ge film. The legend applies to both plots.

parts of Eq. (1) are fitted simultaneously by a least-square procedure which follows the Levenberg-Marquardt algorithm.<sup>34</sup> The procedure was first verified on a reference Ge film grown on a Ge substrate. The critical point parameters for the Ge film were found to be in excellent agreement with the bulk Ge values reflecting the accuracy of our procedure as well as the quality of our Ge film.<sup>22</sup> Figures 3 and 4 show the second derivative of complex dielectric function for  $\text{Ge}_{0.98}\text{Sn}_{0.02}$  and  $\text{Ge}_{0.83}\text{Sn}_{0.17}$  alloys. The standard features in the derivative spectra corresponding to  $E_1$ ,  $E_1 + \Delta_1$ ,  $E'_0$ , and  $E_2$  are clearly identified. The four parameters associated with each critical point are extracted from a fit using Eq. (1).

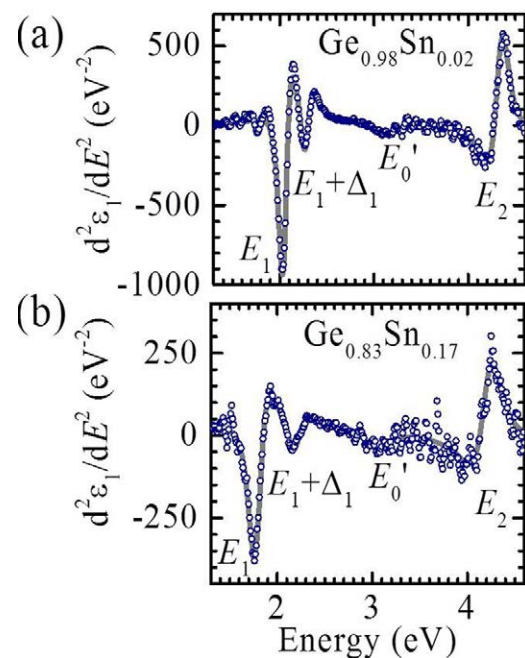


FIG. 3. Numerical second derivatives of real parts of the dielectric function of  $\text{Ge}_{0.98}\text{Sn}_{0.02}$  (top) and  $\text{Ge}_{0.83}\text{Sn}_{0.17}$  (bottom) alloys. Experimental data are plotted in circles and the model is plotted using solid lines.

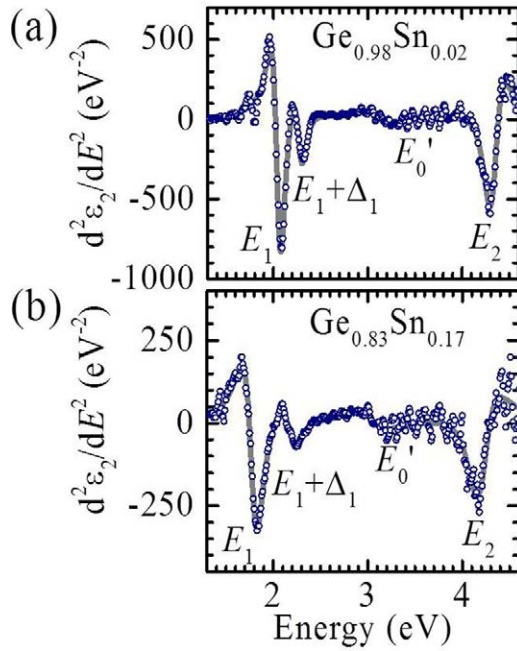


FIG. 4. Numerical second derivatives of imaginary parts of the dielectric function of  $\text{Ge}_{0.98}\text{Sn}_{0.02}$  (top) and  $\text{Ge}_{0.83}\text{Sn}_{0.17}$  (bottom) alloys. Experimental data are plotted in circles and the model is plotted using solid lines.

## IV. RESULTS AND DISCUSSION

### A. $E_1$ and $E_1 + \Delta_1$

The compositional dependence of  $E_1$  and  $E_1 + \Delta_1$  is shown in Figure 5. We have already shown in Ref. 6 that  $E_1$  and  $E_1 + \Delta_1$  in pseudomorphic GeSn can be explained in terms of relaxed GeSn alloys and deformation potential theory using the expressions<sup>35,36</sup>

$$E_1(x, \varepsilon_{\parallel}) = E_1(x) + \Delta_1(x)/2 + E_H - \sqrt{E_S^2 + (\Delta_1(x)/2)^2}, \quad (2)$$

$$(E_1 + \Delta_1)(x, \varepsilon_{\parallel}) = (E_1 + \Delta_1)(x) - \Delta_1(x)/2 + E_H + \sqrt{E_S^2 + (\Delta_1(x)/2)^2}, \quad (3)$$

where  $E_H = (2/\sqrt{3})D_1^1(1 - c_{12}/c_{11})\varepsilon_{\parallel}$  and  $E_S = -\sqrt{(2/3)}D_3^3(1 + 2c_{12}/c_{11})\varepsilon_{\parallel}$  are the energy shifts due to hydrostatic

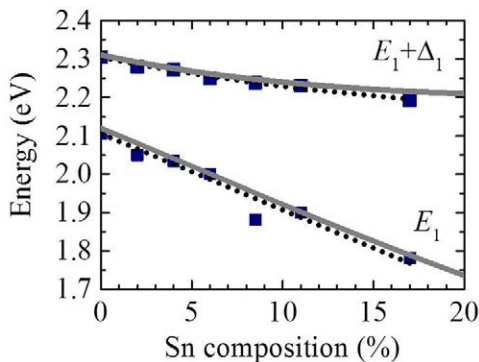


FIG. 5. Compositional dependence of  $E_1$  and  $E_1 + \Delta_1$  in  $\text{Ge}_{1-x}\text{Sn}_x$  alloys. The solid curves  $E_1$  and  $E_1 + \Delta_1$  correspond to Eqs. (2) and (3), respectively, which take into account the compositional dependence of relaxed alloys and strain dependence from deformation potential theory. The dotted curves represent a fit given by Eqs. (4) and (5).

and shear components of strain, respectively.  $D_1^1 = -5.4$  and  $D_3^3 = 3.8$  are the GeSn hydrostatic deformation and shear deformation potentials, respectively.<sup>6</sup>  $c_{12}/c_{11}$  for GeSn is obtained by a linear interpolation between Ge and  $\alpha$ -Sn.<sup>27</sup> The compositional dependence for  $E_1(x)$ ,  $(E_1 + \Delta_1)(x)$ , and  $\Delta_1(x)$  is taken from Ref. 2. Equations (2) and (3) describe experimental  $E_1$  and  $E_1 + \Delta_1$  very well, as shown in Fig. 5. Alternatively, we can also express  $E_1$  and  $E_1 + \Delta_1$  purely in terms of  $x$ . The best fit to  $E_1$  can be described by a linear equation

$$E_1 = 2.11 - (2.0 \pm 0.1)x, \quad (4)$$

whereas  $E_1 + \Delta_1$  can be described by a quadratic expression

$$E_1 + \Delta_1 = 2.30 - (0.91 \pm 0.07)x + (1.6 \pm 0.5)x^2. \quad (5)$$

Both Eqs. (4) and (5) are only valid within  $0 \leq x \leq 17$ . The overall agreement of Eqs. (4) and (5) with Eqs. (2) and (3), respectively, is very good. We note that the coefficients for pseudomorphic GeSn alloys in Eqs. (4) and (5) are higher than their counterparts for SiGe.<sup>37</sup> This behaviour reminds us of the analogous behavior for bowing parameter in relaxed GeSn transitions compared to SiGe.<sup>2</sup>

The compositional dependence of amplitudes for  $E_1$  represented by  $A_{E_1}(x, \varepsilon_{\parallel})$  is shown in Fig. 6(a). The amplitude

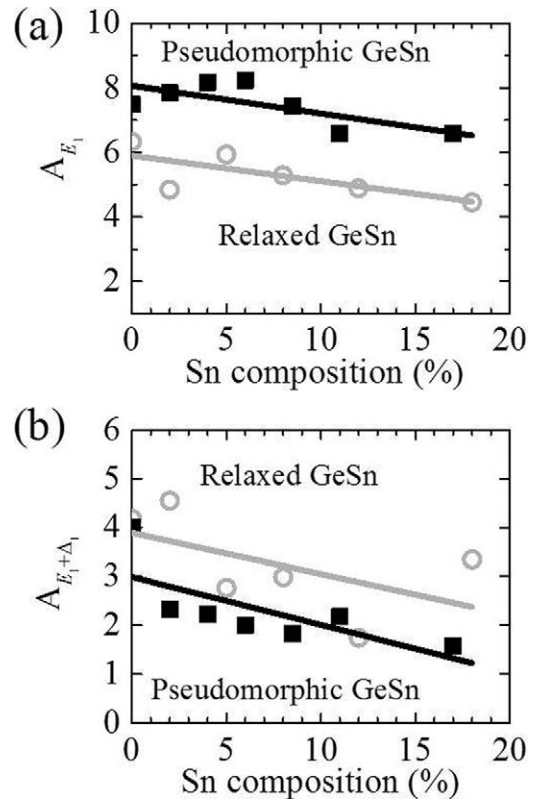


FIG. 6. Compositional dependence of amplitudes for (a)  $E_1$  in pseudomorphic (black squares) and relaxed (gray circles)  $\text{Ge}_{1-x}\text{Sn}_x$  alloys. The solid curves corresponds to linear fits with  $A_{E_1}(x, \varepsilon_{\parallel}) = (8.1 \pm 0.3) - (8.6 \pm 3.5)x$  and  $A_{E_1}(x, 0) = (5.9 \pm 0.4) - (7.9 \pm 3.6)x$ ; and (b)  $E_1 + \Delta_1$  in pseudomorphic (black squares) and relaxed (gray circles)  $\text{Ge}_{1-x}\text{Sn}_x$  alloys. The solid curves corresponds to linear fits with  $A_{E_1 + \Delta_1}(x, \varepsilon_{\parallel}) = (3.0 \pm 0.4) - (9.8 \pm 4.2)x$  and  $A_{E_1 + \Delta_1}(x, 0) = (3.9 \pm 0.6) - (8.4 \pm 6.3)x$ . Amplitudes for relaxed GeSn alloys are taken from Ref. 2.

values for relaxed GeSn alloys denoted by  $A_{E_1}(x, 0)$  are also shown for comparison. Both  $A_{E_1}(x, \varepsilon_{\parallel})$  and  $A_{E_1}(x, 0)$  can be described with a fit linear in  $x$ . The ratio  $\frac{A_{E_1}(x, \varepsilon_{\parallel})}{A_{E_1}(x, 0)}$  is  $>1$  in the entire range of composition studied. Figure 6(b) shows the compositional dependence of amplitudes for  $E_1 + \Delta_1$  denoted by  $A_{E_1 + \Delta_1}(x, \varepsilon_{\parallel})$ . The amplitudes for relaxed alloys,  $A_{E_1 + \Delta_1}(x, 0)$  show large scatter compared to the pseudomorphic alloys but can also be described by a linear fit, as shown in Fig. 6(b). The ratio  $\frac{A_{E_1 + \Delta_1}(x, \varepsilon_{\parallel})}{A_{E_1 + \Delta_1}(x, 0)}$  is  $<1$ . This results in the enhancement of the amplitude ratio of  $E_1$  to  $E_1 + \Delta_1$ ,  $\frac{A_{E_1}(x, \varepsilon_{\parallel})}{A_{E_1 + \Delta_1}(x, \varepsilon_{\parallel})}$ , in our pseudomorphic alloys which was also reported in strained Ge for light polarized parallel to compression axis.<sup>38</sup> Our GeSn alloys possess in-plane compressive strain and the amplitudes are determined from dielectric function which corresponds to in-plane component of the dielectric tensor. We would like to point out that the average value of  $\frac{A_{E_1}(x, 0)}{A_{E_1 + \Delta_1}(x, 0)}$  for relaxed GeSn alloys appears to follow the Ge experimental and theoretical value  $\sim 1.6$ . However, the corresponding amplitude ratio  $\frac{A_{E_1}(x, \varepsilon_{\parallel})}{A_{E_1 + \Delta_1}(x, \varepsilon_{\parallel})}$  for pseudomorphic alloys is  $\sim 3.4:1$ . This ratio is in good agreement with the average amplitude ratio of  $\sim 3.3:1$  found in 1.5–1.7 nm thick pseudomorphic Ge film on Si.<sup>39</sup>

We use the  $k.p$  theory to elucidate whether the presence of strain in our pseudomorphic alloys can cause this behavior in the amplitudes of  $E_1$  and  $E_1 + \Delta_1$ . Theoretical expressions for the amplitudes of  $E_1$  and  $E_1 + \Delta_1$  have been derived for uniaxially strained Ge along [001] for the two cases: (a) light polarized parallel to stress and (b) polarization of light perpendicular to stress.<sup>23,40</sup> Since our alloys are under the influence of biaxial stress, the electric field vector is simultaneously polarized both parallel and perpendicular to stress in the film.<sup>31</sup> For such a case, we can take an average of the amplitudes for each strained transition and express the amplitude ratio as

$$\frac{A_{E_1}(x, \varepsilon_{\parallel})}{A_{E_1}(x, 0)} = 1 + \frac{E_s}{2\Delta_1}, \quad (6)$$

$$\frac{A_{E_1 + \Delta_1}(x, \varepsilon_{\parallel})}{A_{E_1 + \Delta_1}(x, 0)} = 1 - \frac{E_s}{2\Delta_1}. \quad (7)$$

We observe that the above two expressions explain the trend observed for the ratio of amplitudes for  $E_1$  and  $E_1 + \Delta_1$ . Figure 7 shows the amplitude ratios for the two transitions. The theory does not fully explain the experimental data. The agreement with experimental ratio gets better if the direction of stress were nearly parallel to the polarization of light for either critical point. This is in contrast to what has been argued for biaxially strained SiGe and SiGeC alloys where only the case of light polarized perpendicular to the stress direction is assumed to be important.<sup>36,41</sup> Even in the large shear approximation where the spin-orbit splitting is ignored in comparison to  $E_s$ , although not valid in Ge and GeSn, an enhancement ratio of 1.7 is expected for  $\frac{A_{E_1}(\varepsilon)}{A_{E_1 + \Delta_1}(\varepsilon)}$  compared to the observed value of 3.4. A detailed investigation may be

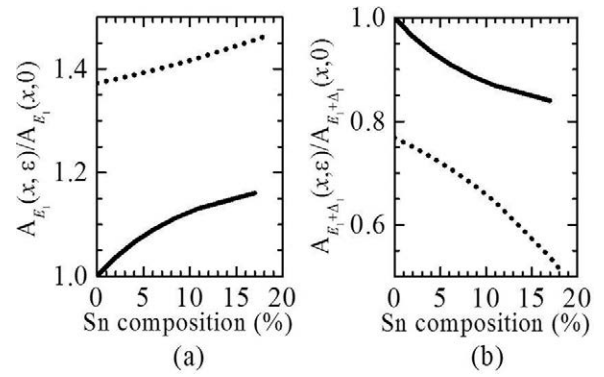


FIG. 7. Compositional dependence of amplitude ratios for  $E_1$  to  $E_1 + \Delta_1$  (a)  $A_{E_1}(x, \varepsilon_{\parallel})/A_{E_1}(x, 0)$  (b)  $A_{E_1 + \Delta_1}(x, \varepsilon_{\parallel})/A_{E_1 + \Delta_1}(x, 0)$ . The solid curve corresponds to experimental ratio, whereas the dotted curve corresponds to  $k.p$  as defined in Eqs. (6) and (7).

necessary to understand the polarization dependence of amplitudes for  $E_1$  and  $E_1 + \Delta_1$  in pseudomorphic GeSn alloys.

The compositional dependence of broadenings for  $E_1$  and  $E_1 + \Delta_1$  is shown in Figs. 8(a) and 8(b), respectively. We fitted the experimental data with a quadratic expression given by

$$\Gamma = \Gamma_{Ge}(1 - x) + \Gamma_{Sn}x - bx(1 - x), \quad (8)$$

where  $\Gamma_{Ge}$  and  $\Gamma_{Sn}$  are the broadening parameters for Ge and  $\alpha$ -Sn, respectively.  $b$  is the bowing parameter. Broadenings for pseudomorphic GeSn alloys clearly lie below the relaxed alloys with  $b$  reduced by nearly half with respect to relaxed

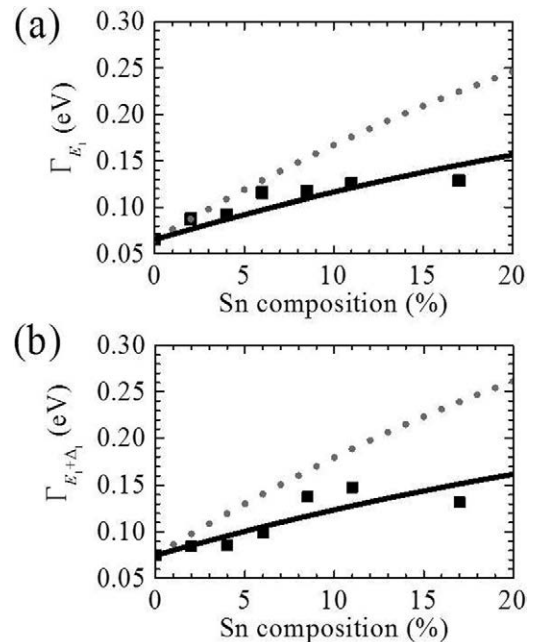


FIG. 8. Compositional dependence of broadening parameter for (a)  $E_1$  in pseudomorphic  $\text{Ge}_{1-x}\text{Sn}_x$  alloys. The dotted curve corresponds to relaxed alloys from Ref. 2. The solid curve is a fit using Eq. (8) with  $\Gamma_{Ge} = 0.066$  eV,  $\Gamma_{Sn} = 0.080$  eV, and  $b = -0.55 \pm 0.06$  eV; and (b)  $E_1 + \Delta_1$  in pseudomorphic  $\text{Ge}_{1-x}\text{Sn}_x$  alloys. The dotted curve corresponds to relaxed alloys from Ref. 2. The solid curve is a fit using Eq. (8) with  $\Gamma_{Ge} = 0.075$  eV,  $\Gamma_{Sn} = 0.087$  eV, and  $b = -0.54 \pm 0.07$  eV.

alloys. The narrower broadenings in all of our alloys could be attributed to the superior structural quality of the strained GeSn alloys compared to relaxed GeSn alloys grown on Si. This behavior is also observed in SiGeC alloys. Relaxed SiGeC films with higher dislocation density show broader  $E_1$  peaks compared to pseudomorphic films. It must be pointed out that FWHM of (004)  $\omega$ -2 $\theta$  scan in the state of the art as-grown relaxed GeSn alloys grown on Si by CVD is approximately six times larger than our pseudomorphic alloys ( $<0.1^\circ$ ) with similar film thickness and composition.<sup>1</sup> Upon annealing, the FWHM of (004)  $\omega$ -2 $\theta$  peak of CVD grown GeSn samples becomes comparable to as-grown pseudomorphic alloys. We expect the broadenings in annealed CVD grown GeSn alloys and MBE grown pseudomorphic alloys to have similar values.

The compositional dependence of phase angle  $\Phi$  for  $E_1$  or  $E_1 + \Delta_1$  transition is shown in Fig. 9.  $\Phi$  is assumed to capture the excitonic effects in Ge.<sup>22</sup> It was found to decrease with temperature and impurity concentration in Ge suggesting a decrease in excitonic effects. The phase angles for all alloys are lower than Ge indicating that the excitonic effects are reduced in GeSn compared to Ge. We obtain  $\Phi \sim 0.64 \pm 0.04$  radians for the pseudomorphic alloys.

## B. $E'_0$ and $E_2$

The compositional dependence of  $E'_0$  and  $E_2$  is shown in Figs. 10 and 11, respectively. The dotted curves correspond to the compositional dependence of relaxed alloys. We observe that both  $E'_0$  and  $E_2$  are blue-shifted with respect to relaxed alloys under the influence of compressive strain. Strain analysis has yet to be established for  $E'_0$  and  $E_2$  even in standard materials such as Ge and SiGe. This is mainly due to the non-availability of reliable deformation potentials for these transitions. As a result we will express the energy shifts due to strain in terms of Sn composition. A quadratic fit is needed to describe the compositional dependence of  $E'_0$  and  $E_2$ . We obtain

$$E'_0 = 3.14 - (1.3 \pm 0.1)x + (4.2 \pm 0.8)x^2, \quad (9)$$

$$E_2 = 4.35 - (0.7 \pm 0.1)x - (1.5 \pm 0.8)x^2. \quad (10)$$

Figures 10 and 11 show the energy shifts caused by strain for  $E'_0$  and  $E_2$ .  $E'_0$  shows larger strain-induced shifts as compared

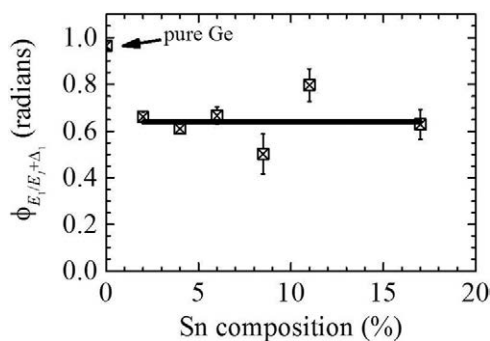


FIG. 9. Compositional dependence of the common phase angles for  $E_1$  and  $E_1 + \Delta_1$ . The solid constant line,  $\Phi = 0.64 \pm 0.04$  gives the best fit to GeSn experimental data.

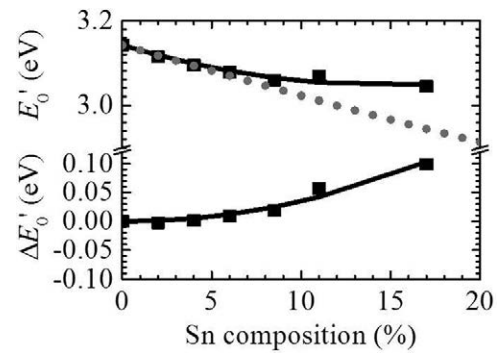


FIG. 10. (a) Compositional dependence of  $E'_0$  in  $\text{Ge}_{1-x}\text{Sn}_x$  alloys. The solid curve represents the best fit given by Eq. (9). The dotted curve corresponds to the compositional dependence of relaxed GeSn alloys from Ref. 2; and (b) Energy shift due to strain for  $E'_0$  expressed in terms of composition. The solid curve represents the difference between Eq. (9) and the compositional dependence in relaxed alloys.

to  $E_2$ . Combining Eqs. (9) and (10) with the compositional dependence of  $E'_0$  and  $E_2$  in relaxed GeSn alloys, we can express the energy shifts due to strain as

$$\Delta E'_0 = -0.0234x + 3.7x^2, \quad (11)$$

$$\Delta E_2 = 0.424x - 1.879x^2. \quad (12)$$

Equations (11) and (12) predict the experimental energy shifts due to strain reasonably well, as shown in Figs. 10 and 11.

The compositional dependence of amplitude for  $E_2$  and  $E'_0$  is shown in Fig. 12. The amplitudes for  $E_2$  appear to decrease linearly with Sn composition whereas the amplitudes for  $E'_0$  essentially retain the same value as that of Ge. Figure 13 shows the compositional dependence of broadening parameters for  $E_2$  and  $E'_0$ . Broadenings for  $E_2$  critical point are also lower compared to relaxed alloys. The broadening parameters associated with  $E'_0$  critical point are very similar to relaxed alloys. The compositional dependence of phase angles for  $E_2$  and  $E'_0$  is shown in Fig. 14. Phase angles for  $E_2$  appear to decrease linearly as a function of Sn composition whereas it appears to retain Ge values for  $E'_0$  in GeSn. It is interesting to note that all the  $E'_0$  critical point

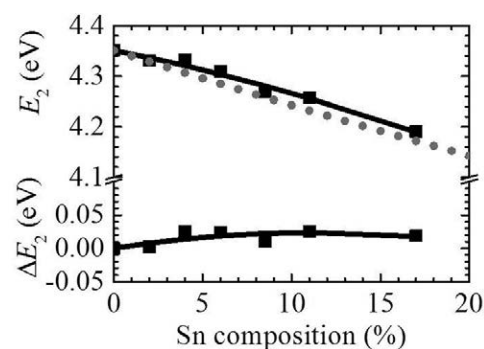


FIG. 11. (a) Compositional dependence of  $E_2$  in  $\text{Ge}_{1-x}\text{Sn}_x$  alloys. The solid curve represents the best fit given by Eq. (10). The dotted curve corresponds to the compositional dependence of relaxed GeSn alloys from Ref. 2; and (b) Energy shift due to strain for  $E_2$  expressed in terms of composition. The solid curve represents the difference between Eq. (10) and the compositional dependence in relaxed alloys.

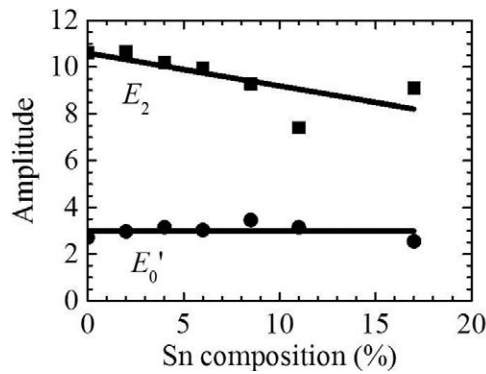


FIG. 12. Compositional dependence of amplitude parameters for  $E'_0$  and  $E_2$  in  $\text{Ge}_{1-x}\text{Sn}_x$  alloys. The amplitude parameter for  $E_2$  shows a linear compositional dependence,  $A_{E_2}(x) = 10.6 - (14.4 \pm 3.4)x$ . The amplitude parameter for  $E'_0$  is nearly constant,  $A_{E'_0}(x) = 3.0 \pm 0.1$ , in the entire compositional range studied.

parameters except the energy parameter are virtually same in both Ge and GeSn.

## V. CONCLUSIONS

The optical critical point parameters of pseudomorphic GeSn alloys grown directly on Ge by MBE were investigated by spectroscopic ellipsometry. We determined the compositional dependence of amplitudes, broadenings, energies, and phase angles for critical points  $E_1$ ,  $E_1 + \Delta_1$ ,  $E'_0$ , and  $E_2$ . The results can be understood in terms of Ge-like electronic bandstructure. Two notable differences are observed between relaxed and pseudomorphic GeSn alloys. Pseudomorphic GeSn alloys show narrower broadening

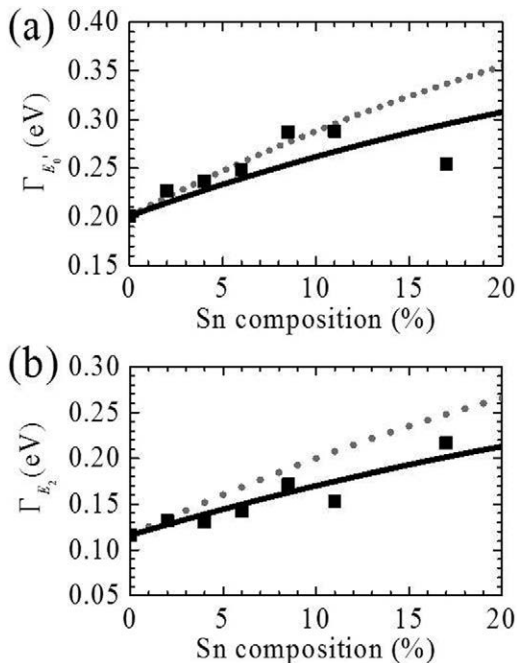


FIG. 13. Compositional dependence of broadening parameters for (a)  $E'_0$  in pseudomorphic  $\text{Ge}_{1-x}\text{Sn}_x$  alloys. The dotted curve corresponds to relaxed alloys from Ref. 2. The solid curve is a fit using Eq. (8) with  $\Gamma_{\text{Ge}} = 0.210$  eV,  $\Gamma_{\text{Sn}} = 0.145$  eV, and  $b = -0.74 \pm 0.12$  eV; and (b)  $E_2$  in pseudomorphic  $\text{Ge}_{1-x}\text{Sn}_x$  alloys. The dotted curve corresponds to relaxed alloys from Ref. 2. The solid curve is a fit using Eq. (8) with  $\Gamma_{\text{Ge}} = 0.116$  eV,  $\Gamma_{\text{Sn}} = 0.144$  eV, and  $b = -0.57 \pm 0.06$  eV.

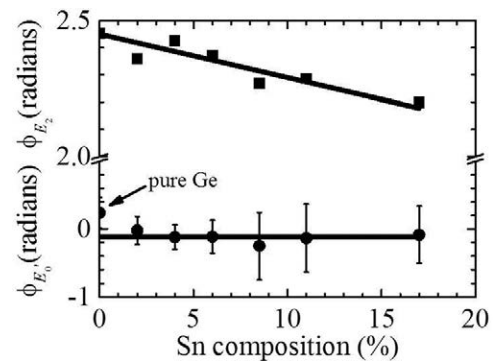


FIG. 14. Compositional dependence of phase angles for  $E'_0$  and  $E_2$  in  $\text{Ge}_{1-x}\text{Sn}_x$  alloys. The phase angle for  $E_2$  shows a linear compositional dependence,  $\Phi_{E_2}(x) = 2.45 - (1.57 \pm 0.16)x$ , whereas the phase angle for  $E'_0$  is nearly constant,  $\Phi_{E'_0}(x) = -0.12 \pm 0.03$ , in the entire compositional range studied.

parameters compared to relaxed alloys indicating lower dislocation density in our pseudomorphic alloys relative to relaxed alloys. The amplitudes for  $E_1$  and  $E_1 + \Delta_1$  in pseudomorphic GeSn appear to show stress dependence with trends described by the  $k \cdot p$  theory, but a thorough investigation may be needed to fully explain the experimental values. All the critical points show lower phase angles compared to Ge suggesting reduction of excitonic effects in GeSn.

## ACKNOWLEDGMENTS

This work was supported by the National Research Foundation under the Competitive Research Programme (Grant No. NRF-CRP6-2010-4).

- <sup>1</sup>G. Grzybowski, R. T. Beeler, L. Jiang, D. J. Smith, J. Kouvetakis, and J. Menéndez, *Appl. Phys. Lett.* **101**(7), 072105 (2012).
- <sup>2</sup>V. R. D'Costa, C. S. Cook, A. G. Birdwell, C. L. Littler, M. Canonico, S. Zollner, J. Kouvetakis, and J. Menendez, *Phys. Rev. B* **73**(12), 125207 (2006).
- <sup>3</sup>B. Vincent, F. Gencarelli, H. Bender, C. Merckling, B. Douhard, D. H. Petersen, O. Hansen, H. H. Henrichsen, J. Meersschaet, W. Vandervorst, M. Heyns, R. Loo, and M. Caymax, *Appl. Phys. Lett.* **99**(15), 152103 (2011).
- <sup>4</sup>N. Bhargava, M. Coppinger, J. P. Gupta, L. Wielunski, and J. Kolodzey, *Appl. Phys. Lett.* **103**(4), 041908 (2013).
- <sup>5</sup>M. Oehme, D. Buca, K. Kosteci, S. Wirths, B. Holländer, E. Kasper, and J. Schulze, *J. Cryst. Growth* **384**, 71 (2013).
- <sup>6</sup>V. R. D'Costa, W. Wang, Q. Zhou, E. S. Tok, and Y.-C. Yeo, *Appl. Phys. Lett.* **104**(2), 022111 (2014).
- <sup>7</sup>H. Lin, R. Chen, W. Lu, Y. Huo, T. I. Kamins, and J. S. Harris, *Appl. Phys. Lett.* **100**(10), 102109 (2012).
- <sup>8</sup>J. P. Gupta, N. Bhargava, S. Kim, T. Adam, and J. Kolodzey, *Appl. Phys. Lett.* **102**(25), 251117 (2013).
- <sup>9</sup>W.-J. Yin, X.-G. Gong, and S.-H. Wei, *Phys. Rev. B* **78**(16), 161203 (2008).
- <sup>10</sup>J. Mathews, R. T. Beeler, J. Tolle, C. Xu, R. Roucka, J. Kouvetakis, and J. Menendez, *Appl. Phys. Lett.* **97**(22), 221912 (2010).
- <sup>11</sup>J. Mathews, R. Roucka, J. Xie, S. Q. Yu, J. Menéndez, and J. Kouvetakis, *Appl. Phys. Lett.* **95**(13), 133506 (2009).
- <sup>12</sup>M. Oehme, M. Schmid, M. Kaschel, M. Gollhofer, D. Widmann, E. Kasper, and J. Schulze, *Appl. Phys. Lett.* **101**(14), 141110 (2012).
- <sup>13</sup>S. Su, B. Cheng, C. Xue, W. Wang, Q. Cao, H. Xue, W. Hu, G. Zhang, Y. Zuo, and Q. Wang, *Opt. Express* **19**(7), 6400 (2011).
- <sup>14</sup>G. Han, S. Su, C. Zhan, Q. Zhou, Y. Yang, L. Wang, P. Guo, W. Wei, C. P. Wong, Z. X. Shen, B. Cheng, and Y. C. Yeo, *IEEE Int. Electron Devices Meet.* **2011**, 16.7.1.
- <sup>15</sup>S. Gupta, B. Vincent, B. Yang, D. Lin, F. Gencarelli, J. Y. J. Lin, R. Chen, O. Richard, H. Bender, B. Magyari-Kope, M. Caymax, J. Dekoster, Y. Nishi, and K. C. Saraswat, *IEEE Int. Electron Devices Meet.* **2012**, 16.2.1.

- <sup>16</sup>X. Gong, G. Han, F. Bai, S. Su, P. Guo, Y. Yang, R. Cheng, D. Zhang, G. Zhang, C. Xue, B. Cheng, J. Pan, Z. Zhang, E. S. Tok, D. Antoniadis, and Y. C. Yeo, *IEEE Electron Device Lett.* **34**(3), 339 (2013).
- <sup>17</sup>C. Eckhardt, K. Hummer, and G. Kresse, *Phys. Rev. B* **89**(16), 165201 (2014).
- <sup>18</sup>A. A. Tonkikh, C. Eisenschmidt, V. G. Talalaev, N. D. Zakharov, J. Schilling, G. Schmidt, and P. Werner, *Appl. Phys. Lett.* **103**(3), 032106 (2013).
- <sup>19</sup>O. Gurdal, P. Desjardins, J. R. A. Carlsson, N. Taylor, H. H. Radamson, J. E. Sundgren, and J. E. Greene, *J. Appl. Phys.* **83**(1), 162 (1998).
- <sup>20</sup>R. Ragan and H. A. Atwater, *Appl. Phys. Lett.* **77**(21), 3418 (2000).
- <sup>21</sup>H. Perez Ladron de Guevara, A. G. Rodriguez, H. Navarro-Contreras, and M. A. Vidal, *Appl. Phys. Lett.* **84**(22), 4532 (2004).
- <sup>22</sup>L. Viña, S. Logothetidis, and M. Cardona, *Phys. Rev. B* **30**(4), 1979 (1984).
- <sup>23</sup>P. Etchegoin, J. Kircher, M. Cardona, and C. Grein, *Phys. Rev. B* **45**, 11721 (1992).
- <sup>24</sup>K. E. Junge, R. Lange, J. M. Dolan, S. Zollner, M. Dashiell, B. A. Orner, and J. Kolodzey, *Appl. Phys. Lett.* **69**(26), 4084 (1996).
- <sup>25</sup>S. Albrecht, L. Reining, R. Del Sole, and G. Onida, *Phys. Rev. Lett.* **80**(20), 4510 (1998).
- <sup>26</sup>J. M. Hartmann, A. M. Papon, V. Destefanis, and T. Billon, *J. Cryst. Growth* **310**(24), 5287 (2008).
- <sup>27</sup>O. Madelung, in *Landolt-Börnstein: Numerical Data and Functional Relationships in Science and Technology*, edited by O. Madelung (Springer-Verlag, Berlin, 1985), Vol. 22a.
- <sup>28</sup>J. A. Woollam, B. D. Johs, C. M. Herzinger, J. N. Hilfiker, R. A. Synowicki, and C. L. Bungay, in *Optical Metrology*, edited by G. A. Al-Jumaily (Denver, Colorado, 1999), Vol. CR72, p. 3.
- <sup>29</sup>Y. Z. Hu, J. T. Zettler, S. Chongsawangvirod, Y. Q. Wang, and E. A. Irene, *Appl. Phys. Lett.* **61**(9), 1098 (1992).
- <sup>30</sup>D. E. Aspnes, *J. Opt. Soc. Am.* **70**(10), 1275 (1980).
- <sup>31</sup>C. J. Vineis, *Phys. Rev. B* **71**(24), 245205 (2005).
- <sup>32</sup>A. Savitzky and M. J. E. Golay, *Anal. Chem.* **36**, 1627 (1964).
- <sup>33</sup>J. Steiner, Y. Termonia, and J. Deltour, *Anal. Chem.* **44**, 1906 (1972).
- <sup>34</sup>W. H. Press, S. A. Teukolsky, W. T. Vetterling, and B. P. Flannery, *Numerical Recipes in C: The Art of Scientific Computing*, 2nd ed. (Cambridge University Press, New York, 1992).
- <sup>35</sup>F. H. Pollak, in *Semiconductors and Semimetals*, edited by P. P. Thomas (Elsevier, 1990), Vol. 32, p. 17.
- <sup>36</sup>S. T. Pantelides and S. Zollner, in *Optoelectronic Properties of Semiconductors and Superlattices*, edited by M. O. Manasreh (Taylor & Francis, New York, 2002), Vol. 15, p. 538.
- <sup>37</sup>R. T. Carline, C. Pickering, D. J. Robbins, W. Y. Leong, A. D. Pitt, and A. G. Cullis, *Appl. Phys. Lett.* **64**(9), 1114 (1994).
- <sup>38</sup>U. Gerhardt, *Phys. Rev. Lett.* **15**(9), 401 (1965).
- <sup>39</sup>J. L. Freeouf, J. C. Tsang, F. K. LeGoues, and S. S. Iyer, *Phys. Rev. Lett.* **64**(3), 315 (1990).
- <sup>40</sup>F. H. Pollak and M. Cardona, *Phys. Rev.* **172**(3), 816 (1968).
- <sup>41</sup>G. Raja Muthinti, M. Medikonda, T. Adam, A. Reznicek, and A. C. Diebold, *J. Appl. Phys.* **112**(5), 053519 (2012).